IEEE Access
Multidisciplinary ⋮ Rapid Review ⋮ Open Access Journal

Received 14 November 2023, accepted 29 November 2023, date of publication 5 December 2023,
date of current version 15 December 2023.

Digital Object Identifier 10.1109/ACCESS.2023.3339856

RESEARCH ARTICLE

Tracking an Underwater Target in a Large Surveillance Region With Sensor Location Uncertainty

VED PRAKASH DUBEY[1], **JOYDEB SAHA**[1], **SHOVAN BHAUMIK**[1], **AND ARITRO DEY**[2], **(Member, IEEE)**

[1]Indian Institute of Technology Patna, Patna, Bihar 801106, India
[2]National Institute of Technology Durgapur, Durgapur, West Bengal 713213, India

Corresponding author: Ved Prakash Dubey (ved_1921ee10@iitp.ac.in)

The work of Joydeb Saha was supported by the Ministry of Education, Government of India, through the Prime Minister's Research Fellowship Scheme under Grant 2702440.

ABSTRACT This paper provides an integrated solution of sensor selection and multi-sensor tracking to localize an underwater target using passive angle-only measurements received from sonobuoys, floating in a large surveillance region. It is evident that sonobuoys, airdropped in the surveillance region, undergo drift due to the influence of sea currents. To accurately capture this behavior, the positions of the sonobuoys are modeled using a stochastic difference equation. Due to some physical limitations, only a few selected sensors are allowed to send the measurement data for an interval of time, and they are chosen by solving an optimization problem whose cost function is formulated based on the Fisher information matrix. The effect of uncertainty in sensor location on measurement noise covariance matrix is calculated and the shifted Rayleigh filter (SRF) is modified so that it can be applied to a system with a nonlinear process model. The combined method of sensor selection and target localization is used to track a target moving in (i) a nearly straight path, and (ii) taking a turn with a constant but unknown turn rate. The tracking performance of the developed method is compared with the conventional Gaussian filters in terms of root mean square error (RMSE), averaged normalized estimation error squared (ANEES), percentage of track divergence, and execution time. The proposed methodology with the SRF provides an improved result when other existing Gaussian filters are compared.

INDEX TERMS Bearing only tracking, fisher information matrix (FIM), sensor management, shifted rayleigh filter, underwater target localization.

I. INTRODUCTION

For underwater surveillance, tracking algorithms play a significant role, and passive tracking is preferred for its stealth feature. To track an underwater object, a single sensor bearing only tracking (BOT) is prevalent in literature [1], [2], [3], [4]. However, for a target following a straight line motion, single sensor system suffers from observability issues [1], [5] and therefore maneuvering the observer is indispensable [6], [7]. To overcome the limitation of the single sensor system and improve the tracking performance, a multi-sensor tracking system is advocated [8], [9], [10].

This paper considers that many battery-powered sonobuoys are airdropped over the water surface in the surveillance region. These sensors are assumed to be distributed uniformly, and they are passive sonar which measures the direction of arrival of a sound signal generated by an underwater target moving in the surveillance region. Further, we consider a centralized network architecture approach [11], [12] in which all the sensors send data to a central fusion center where the tracking algorithms are being run to locate the target. However, due to the constraint of communication bandwidth, it is not always possible to send all sensors' measurement data together. Further, due to the limited battery power of the sensors, it is not practical to set all the sensors always in active transmitting mode. So, at any point during

The associate editor coordinating the review of this manuscript and approving it for publication was Manuel Rosa-Zurera.

tracking, a user-defined number of sensors are allowed to send data to the central processing unit.

The method of sensor selection is available in the literature with other different names *viz.*, sensor management [13], optimal sensor selection [14], and sensor control [15]. A thorough research work has been carried out in [16], [17], and [18] for optimal placement of sensors to track a target. In order to select a predefined number of sensors from which accurate tracking can be achieved, we adopt the approach of [13] and [19] and formulate a cost function based on the FIM. The optimization problem has been solved with the local search method [20]. As the target location is not known to the designer, a prior estimate is used before we formulate the cost function.

In a real-time scenario, the position of the aircraft is known with GPS, and at that point, as the angle of release and the wind velocity direction is known, the initial hitting point of sonobuoys to the sea surface is known with some uncertainty. Further, they are subjected to drift due to sea currents and to address that, we need to model the sensor motion [21]. As both the sensor location and measurements have uncertainty, a modified noise parameter is calculated for various tracking filters including the SRF. The developed tracking methods estimate not only the states of the target but also the location of the sensors. By estimating both the sensor states and the target states simultaneously, we can improve the applicability and accuracy of the tracking system, ultimately leading to better performance in real-world applications. Similar interests for sensor location uncertainty are also found in recent literature for tracking multitarget in radar network [22], imaging [23], and localization [24].

In this work, tracking and sensor selection algorithms are co-designed with the existing Gaussian filters. Two different scenarios have been addressed *viz.* (i) the target moves at a nearly constant velocity in a particular direction, (ii) the target executes a maneuver with a constant but unknown turn rate. Amongst the well known nonlinear filters, the extended Kalman filter (EKF) [25] is widely used but it has limited accuracy. Sigma point Kalman filters such as cubature Kalman filter (CKF) [26], cubature quadrature Kalman filter (CQKF) [27], unscented Kalman filter (UKF) [28], Gauss-Hermite filter (GHF) [29] are the preferred alternatives of the EKF as they overcome the shortcomings of the EKF. Moreover, for BOT, SRF [30], [31] is reported to improve estimation performance. As in the second case, the system dynamics is nonlinear, the SRF is modified with the deterministic sample points during the process update step. A comparative study of conventional Gaussian filters with the modified SRF has been made. The SRF is found to exhibit a superior performance over its competing algorithms as evaluated in terms of root mean square error (RMSE), track divergence, and computation time. Salient contributions to this paper are enlisted below:

i. Consideration of drift in the sensor location due to ocean current and uncertainty.
ii. Selection of cost function based on FIM with the consideration of drift and uncertainty in the sensor location.
iii. Modifying the SRF so that it can be applied to a nonlinear process.
iv. Co-design of sensor selection and target tracking algorithms.
v. Performance comparison of the proposed SRF with the conventional filters in terms of performance metrics.

The remaining part of the paper is organized as follows: The tracking problem with multiple sensors is formulated in Section II. Section III derives an expression of equivalent measurement noise covariance matrix for different filters to incorporate the effect of sensor location uncertainty. Different sensor selection criteria and their solutions are presented in Section IV. An algorithm is presented for tracking along with sensor selection in Section V. The simulation results are reported in Section VI, and the paper ends with a conclusion.

II. PROBLEM FORMULATION

A. PROCESS MODEL OF THE TARGET

1) SCENARIO 1

In this scenario, the target moves in a straight line with a nearly constant velocity [32]. The process equation is given by

$$X_{k+1}^t = FX_k^t + \eta_k, \tag{1}$$

where $X_k^t = \left[x_k^t\ \dot{x}_k^t\ y_k^t\ \dot{y}_k^t\right]^\tau$ is a target state vector. x_k, y_k are positions along X and Y axis, respectively at time step k. F is the system matrix which can be expressed as $F = \text{diag}([F_1,\ F_1])$, where $F_1 = \begin{bmatrix} 1 & T \\ 0 & 1 \end{bmatrix}$, and T is the sampling interval. η_k is the process noise which is assumed to be white, Gaussian with zero mean and covariance Q_k^t *i.e.* $\eta_k \sim \mathcal{N}(0, Q_k^t)$. The expression of Q_k^t is

$$Q_k^t = \text{diag}([Q1,\ Q1]), \tag{2}$$

where $Q1 = \bar{q}_1 \begin{bmatrix} \frac{T^3}{3} & \frac{T^2}{2} \\ \frac{T^2}{2} & T \end{bmatrix}$, and $\bar{q}_1$ is the intensity of process noise.

2) SCENARIO 2

In this scenario, the target moves in a coordinated turn (CT) [33] model in the $x - y$ plane with a nearly constant turn rate. The process model is given by

$$X_{k+1}^t = f(X_k^t) + \eta_k = F(\omega_k)X_k^t + \eta_k, \tag{3}$$

where $X_k^t = \left[x_k^t\ \dot{x}_k^t\ y_k^t\ \dot{y}_k^t\ \omega_k\right]^\tau$, ω_k is the angular turn rate of the target and the expression of F is given by

$$F = \begin{bmatrix} 1 & \frac{\sin\omega_k T}{\omega_k} & 0 & \frac{-(1-\cos\omega_k T)}{\omega_k} & 0 \\ 0 & \cos\omega_k T & 0 & -\sin\omega_k T & 0 \\ 0 & \frac{-(1-\cos\omega_k T)}{\omega_k} & 1 & \frac{-\sin\omega_k T}{\omega_k} & 0 \\ 0 & \sin\omega_k T & 0 & \cos\omega_k T & 0 \\ 0 & 0 & 0 & 0 & 1 \end{bmatrix}. \tag{4}$$

The process noise covariance matrix Q_k^t corresponding to this system is given by $Q_k^t = \text{diag}([\bar{q}_1 Q2,\ \bar{q}_2 T])$, where

$$Q2 = \begin{bmatrix} \frac{2s_{\omega_k}}{\omega_k^3} & \frac{c_{\omega_k}T}{\omega_k^2} & 0 & \frac{s_{\omega_k}}{\omega_k^2} \\ \frac{c_{\omega_k}}{\omega_k^2} & T & -\frac{s_{\omega_k}}{\omega_k^2} & 0 \\ 0 & -\frac{s_{\omega_k}}{\omega_k^2} & \frac{2s_{\omega_k}}{\omega_k^3} & \frac{c_{\omega_k}}{\omega_k^2} \\ \frac{s_{\omega_k}}{\omega_k^2} & 0 & \frac{c_{\omega_k}}{\omega_k^2} & T \end{bmatrix}, \tag{5}$$

where $s_{\omega_k} = \omega_k T - \sin \omega_k T$, $c_{\omega_k} = 1 - \cos \omega_k T$ and $\bar{q}_2$ is the process noise intensity corresponding to its turn rate.

B. MEASUREMENT MODEL

In both scenarios, each sensor provides a bearing angle of the target with reference to its own position. The mathematical model of the i-th sensor's measurement at k-th instant is given by

$$\mathcal{Y}_{k,i} = \theta_{k,i} + w_{k,i}, \quad i = 1, \cdots, n_s, \tag{6}$$

$$\theta_{k,i} = h(X_k^t, X_{k,i}^s) = \tan^{-1}\left(\frac{x_k^t - x_{k,i}^s}{y_k^t - y_{k,i}^s}\right), \tag{7}$$

where θ_k is all the four quadrants' true bearing angle of the target to the sensor; so $\theta_k \in [-\pi, \pi)$ and n_s is the total number of sensors. The sensor state vector is $X_{k,i}^s = [x_{k,i}^s,\ \dot{x}_{k,i}^s,\ y_{k,i}^s,\ \dot{y}_{k,i}^s]^\tau$, and $w_{k,i}$ is an additive noise associated with i-th sensor measurement. This measurement noise is also assumed as white, Gaussian with zero mean and covariance $R_{k,i}$ *i.e.* $\mathbb{E}[w_{k,i}^2] = R_{k,i}$. At a particular time instant, the tracker selects only n number of sensors out of n_s available sensor set and these selected sensors send their measurement to the tracker. So, at a time instant k, the measurement received by the tracker is given by

$$\mathcal{Y}_k = \left[\mathcal{Y}_{k,1}, \ \cdots, \ \mathcal{Y}_{k,n}\right]^\tau. \tag{8}$$

C. MODELING OF SEA CURRENT

The sensors are floating on the surface of the water, and due to external forces such as intensive wind velocity and ocean currents, their positions are drifting with time. This uncertain position of sensors can be modelled by a random walk [34], [35] and its state equation is represented by

$$X_{k+1,i}^s = FX_{k,i}^s + v_{k,i}, \quad i = 1, \cdots, n_s, \tag{9}$$

where F is a sensor transition matrix, $v_{k,i}$ is the process noise associated with the sensor position to compensate for the external disturbance. The sensor process noise is assumed as white, Gaussian with zero mean and covariance $Q_{k,i}^s$ *i.e.* $v_{k,i} \sim \mathcal{N}(0, Q_{k,i}^s)$ and mutually independent with other sensor states. The sensors are deployed from a moving platform (such as airplane), and the initial sensor location is assumed to be $X_{0,i}^s \sim \mathcal{N}(\bar{X}_{0,i}^s, P_{0,i}^s)$, $i = 1, \cdots, n_s$. The initial sensor state mean is $\bar{X}_{0,i}^s$, and the related covariance matrix is $P_{0,i}^s$.

III. EQUIVALENT MEASUREMENT NOISE COVARIANCE

The measurement equation for each sensor is a nonlinear function of target and sensor states. Sensors are floating on the sea surfaces and they drift due to ocean currents, and their location becomes uncertain. This uncertainty in the sensors' position leads to an additional error while estimating the target states. To incorporate such an effect in our estimation, equivalent measurement error covariance is required to calculate. Without loss of generality, here we consider a single sensor measurement to derive the expression for equivalent covariance. Let us consider the measurement of i-th sensor at k-th instant *i.e.*

$$\mathcal{Y}_{k,i} = h(X_k^t, X_{k,i}^s) + w_{k,i}.$$

As the true position of sonobuoy is unknown, we replace it with the estimated position and thus the measurement equation becomes

$$\mathcal{Y}_{k,i} = h(X_k^t, \hat{X}_{k|k-1,i}^s) + e_{\mathcal{Y}_{k,i}}^s + w_{k,i}, \tag{10}$$

where $\hat{X}_{k|k-1,i}^s$ is the prior position of the i-th sensor and the term $e_{\mathcal{Y}_{k,i}}^s$ is an additional error in measurement due to uncertainty in sensor position. We can write the above equation as

$$\mathcal{Y}_{k,i} = h(X_k^t, \hat{X}_{k|k-1,i}^s) + w'_{k,i},$$

where $w'_{k,i}$ is the updated measurement noise constructed by incorporating the effect of sensor location uncertainty with mean zero and covariance $\mathbb{E}[w'^2_{k,i}] = \hat{R}_{k,i}$.

The expression of $\hat{R}_{k,i}$ will depend on the choice of the filter used for estimation. In the following three Lemmas, we provide the final expression of resultant or equivalent measurement noise covariance when the estimators are the EKF, deterministic sample point filters, and the SRF, respectively. Although, the final expressions of $\hat{R}_{k,i}$ for the EKF and sampling point filters are available in literature [35], we provide a proof in Lemma 1 and 2 for completeness of the work.

Lemma 1: In the extended Kalman filter (EKF), the equivalent measurement noise covariance matrix is expressed as

$$\hat{R}_{k,i} = H_{k,i} P_{k|k-1,i}^s H_{k,i}^\tau + R_{k,i}, \tag{11}$$

where $H_{k,i} = \dfrac{\partial h(X_k^t, X_{k,i}^s)}{\partial X_{k,i}^s}\Big|_{X_{k,i}^s = \hat{X}_{k|k-1,i}^s}$ *is the Jacobian matrix, and* $P_{k|k-1,i}^s$ *is the predicted error covariance matrix of i-th sensor.*

Proof: From (10) substituting the error expression,

$$\begin{aligned} \mathcal{Y}_{k,i} &\approx h(X_k^t, \hat{X}_{k|k-1,i}^s) + H_{k,i}^s(X_{k,i}^s - \hat{X}_{k|k-1,i}) + w_{k,i}, \\ &= h(X_k^t, \hat{X}_{k|k-1,i}^s) + H_{k,i}^s \tilde{X}_{k|k-1,i}^s + w_{k,i}, \\ &= h(X_k^t, \hat{X}_{k|k-1,i}^s) + w'_{k,i}, \end{aligned}$$

where $w'_{k,i} = H^s_{k,i}\tilde{X}^s_{k|k-1,i} + w_{k,i}$, with $\mathbb{E}[w'_{k,i}] = 0$ and covariance

$$\begin{aligned}\hat{R}_{k,i} &= \mathbb{E}[w'^2_{k,i}]\\ &= \mathbb{E}[(H^s_{k,i}\tilde{X}^s_{k|k-1,i} + w_{k,i})(H^s_{k,i}\tilde{X}^s_{k|k-1,i} + w_{k,i})^\tau]\\ &= \mathbb{E}[H^s_{k,i}\tilde{X}^s_{k|k-1}\tilde{X}^{s^\tau}_{k|k-1,i}H^{s^\tau}_{k,i} + w^2_{k,i}]\\ &= H^s_{k,i}P^s_{k|k-1,i}H^{s^\tau}_{k,i} + R_{k,i}.\end{aligned}$$

■

Lemma 2: In deterministic sample point filters, the expression for the equivalent measurement noise covariance matrix is expressed as

$$\hat{R}_{k,i} = \sum_{j=1}^{n_p} W_j(\mathcal{Y}^s_{k|k-1,j} - \hat{\mathcal{Y}}^s_{k|k-1})^2 + R_{k,i}, \tag{12}$$

where n_p is the total number of deterministic sample points, W_j and $\mathcal{Y}^s_{k|k-1,j}$ are j-th weight and predictive measurements respectively. $\hat{\mathcal{Y}}^s_{k|k-1}$ is the mean of predictive measurements.

Proof: Sample points are generated by

$$\hat{\mathcal{X}}^s_{k|k-1,j} = \hat{X}^s_{k|k-1,i} + S^s_{k|k-1}\xi_j, \quad j = 1, \cdots, n_p,$$

where $P^s_{k|k-1,i} = S^s_{k|k-1}S^{s^\tau}_{k|k-1}$, and ξ is a set of support points for unity covariance matrix. Expected measurements are $\hat{\mathcal{Y}}^s_{k|k-1} = \sum_{j=1}^{n_p} W_j\mathcal{Y}^s_{k|k-1,j}$, where $\mathcal{Y}^s_{k|k-1,j} = h(\hat{X}_{t,k|k-1}, \hat{\mathcal{X}}^s_{k|k-1,j})$. The errors for a nonlinear system is, $e^s_{\mathcal{Y}_{k,i}} = \mathcal{Y}^s_{k|k-1} - \hat{\mathcal{Y}}^s_{k|k-1} = \tilde{\mathcal{Y}}^s_{k|k-1}$ and from (10)

$$\begin{aligned}\mathcal{Y}_{k,i} &= h(X^t_k, \hat{X}^s_{k|k-1,i}) + \tilde{\mathcal{Y}}^s_{k|k-1} + w_{k,i},\\ &= h(X^t_k, \hat{X}^s_{k|k-1,i}) + w'_{k,i},\end{aligned}$$

where $w'_{k,i} = \tilde{\mathcal{Y}}^s_{k|k-1} + w_{k,i}$, with $\mathbb{E}[w'_{k,i}] = 0$ and covariance

$$\begin{aligned}\hat{R}_{k,i} &= \mathbb{E}[w'^2_{k,i}] = \mathbb{E}[(\tilde{\mathcal{Y}}_{k|k-1} + w_{k,i})^2] = \mathbb{E}[\tilde{\mathcal{Y}}^{s^2}_{k|k-1} + w^2_{k,i}]\\ &= \sum_{j=1}^{n_p} W_j(\mathcal{Y}^s_{k|k-1,j} - \hat{\mathcal{Y}}^s_{k|k-1})^2 + R_{k,i}.\end{aligned}$$

■

The SRF is a superior filtering technique commonly used in BOT applications. This filter transforms the original measurement into the relative position of the target to the sensor and then uses the transformed measurement to track the target. To design the SRF, the uncertainty of sensor location is directly incorporated into the transformed measurement instead of the original measurement. This approach yields better accuracy and is widely documented in the literature.

Lemma 3: In the SRF, the covariance matrix of the transformed measurement, $\mathcal{Y}_{k,i}$, is estimated as

$$\begin{aligned}\hat{R}_{k,i} = \{||H(\hat{X}^t_{k|k-1} - \hat{X}^s_{k|k-1,i})||^2 + trace(HP^t_{k|k-1}H^\tau)\\ + trace(HP^s_{k|k-1,i}H^\tau)\}R_{k,i}I_{2\times 2} + HP^s_{k|k-1,i}H^\tau,\end{aligned} \tag{13}$$

where $H = \begin{bmatrix}1 & 0 & 0 & 0\\ 0 & 0 & 1 & 0\end{bmatrix}$.

Proof: Consider the measurement of i-th sensor at k-th step

$$\mathcal{Y}_{k,i} = h(X^t_k, X^s_{k,i}) + w_{k,i}.$$

The measurement $\mathcal{Y}_{k,i}$ is transformed to relative position target to the sensor *i.e.* given by

$$Z_{k,i} = HX_{k,i} + \rho_{k,i}, \tag{14}$$

where relative state vector $X_{k,i} = X^t_k - X^s_{k,i}$ and $\rho_{k,i}$ is transformed noise of $w_{k,i}$ with mean $\mathbb{E}[\rho_{k,i}] = 0$ and covariance

$$Q^m_{k,i} = \mathbb{E}[\rho_{k,i}\rho^\tau_{k,i}] = \begin{bmatrix}\sigma^2_{x_k} & \sigma_{x_k y_k}\\ \sigma_{y_k x_k} & \sigma^2_{y_k}\end{bmatrix}.$$

By assuming same variance in both x and y position, $\sigma_{x_k} = \sigma_{y_k} = \sigma_{k,i}$ and both of them are uncorrelated *i.e.* $\sigma_{x_k,y_k} = 0$,

$$Q^m_{k,i} = \begin{bmatrix}\sigma^2_{k,i} & 0\\ 0 & \sigma^2_{k,i}\end{bmatrix} = \sigma^2_{k,i}I_{2\times 2}. \tag{15}$$

The measurement $\mathcal{Y}_{k,i} = h(X_{k,i}) + w_{k,i}$, and its noise free measurement is given by $\mathcal{Y}_{k,i} = h(X_{k,i}) = \tan^{-1}(\frac{x_k}{y_k})$, where $x_k = x^t_k - x^s_{k,i}$, $y_k = y^t_k - y^s_{k,i}$. By differentiating the above equation

$$\Delta\mathcal{Y}_{k,i} = \frac{y_k}{x^2_k + y^2_k}\Delta x_k - \frac{x_k}{x^2_k + y^2_k}\Delta y_k.$$

Covariance of $\mathcal{Y}_{k,i}$ is given by

$$\begin{aligned}R_{k,i} &= \mathbb{E}[\Delta\mathcal{Y}^2_{k,i}] = \mathbb{E}[(\frac{y_k}{x^2_k + y^2_k})^2\Delta x^2_k + (\frac{x_k}{x^2_k + y^2_k})^2\Delta y^2_k]\\ &= \mathbb{E}[\frac{1}{x^2_k + y^2_k}]\sigma^2_{k,i},\end{aligned}$$

or,

$$\sigma^2_{k,i} = \mathbb{E}[x^2_k + y^2_k]R_{k,i} = (\hat{x}^2_k + \hat{y}^2_k + P_{x_k x_k} + P_{y_k y_k})R_{k,i}. \tag{16}$$

By substituting $P_{x_k x_k} = P^t_{x_k x_k} + P^s_{x_k x_k}$, and $P_{y_k y_k} = P^t_{y_k y_k} + P^s_{y_k y_k}$ in (16),

$$\begin{aligned}\sigma^2_{k,i} = \{||H(\hat{X}^t_{k|k-1} - \hat{X}^s_{k|k-1,i})||^2 + \text{trace}(HP^t_{k|k-1}H^\tau)\\ + \text{trace}(HP^s_{k|k-1,i}H^\tau)\}R_{k,i}.\end{aligned}$$

By substituting the value of $\sigma^2_{k,i}$ in (15), the covariance of transformed measurement is obtained by

$$\begin{aligned}Q^m_{k,i} = \{||H(\hat{X}^t_{k|k-1} - \hat{X}^s_{k|k-1})||^2 + \text{trace}(HP^t_{k|k-1}H^\tau)\\ + \text{trace}(HP^s_{k|k-1,i}H^\tau)\}R_{k,i}I_{2\times 2}.\end{aligned} \tag{17}$$

By taking the transformed measurement from (14)

$$\begin{aligned}Z_{k,i} &= H(X^t_k - X^s_{k,i}) + \rho_{k,i},\\ &= H(X^t_k - \{\hat{X}^s_{k|k-1,i} + \tilde{X}^s_{k|k-1,i}\}) + \rho_{k,i},\\ &= H(X^t_k - \hat{X}^s_{k|k-1,i}) + \rho'_{k,i},\end{aligned}$$

where the updated noise $\rho'_{k,i} = \rho_{k,i} - H\tilde{X}^s_{k|k-1,i}$ with mean $\mathbb{E}[\rho'_{k,i}] = 0$ and covariance

$$\begin{aligned}\hat{R}_{k,i} &= \mathbb{E}[\rho'_{k,i}\rho'^{\tau}_{k,i}],\\ &= \mathbb{E}[(\rho_{k,i} - H\tilde{X}^s_{k|k-1,i})(\rho_{k,i} - H\tilde{X}^s_{k|k-1,i})^\tau],\\ &= \mathbb{E}[\rho_{k,i}\rho^\tau_{k,i} + H\tilde{X}^s_{k|k-1,i}\tilde{X}^{s^\tau}_{k|k-1,i}H^\tau],\\ &= Q^m_{k,i} + HP^s_{k|k-1,i}H^\tau,\\ &= \{||H(\hat{X}^t_{k|k-1} - \hat{X}^s_{k|k-1,i})||^2 + \mathrm{trace}(HP^t_{k|k-1}H^\tau)\\ &+ \mathrm{trace}(HP^s_{k|k-1,i}H^\tau)\}R_{k,i}I_{2\times2} + HP^s_{k|k-1,i}H^\tau.\end{aligned}$$

■

IV. SELECTION OF SENSORS

A. COST FUNCTIONS

For effective sensor management, a sensor selection algorithm needs to be incorporated with the tracking algorithm. Towards this objective, different cost functions have been proposed in the earlier literature [13] and [19] based on Euclidean distance (ED) and the FIM. By optimizing the cost functions, the tracker selects a user-specified number of sensors that have the capability to provide accurate tracking.

1) ED-BASED COST FUNCTION

The predicted distance between each sensor and the target is computed to generate the cost function. Let S_i represents the selection status of the sensor. If the i^{th} sensor is selected, then $S_i = 1$ otherwise set to be 0, so $S_i \in \{0, 1\}$, and S^*_k is an optimal status of sensor set, given by

$$\begin{aligned}S^*_k = \arg\min_{S_i} \sum_{i=1}^{n_s} S_i\{(\hat{x}^t_{k|k-1} - \hat{x}^s_{k|k-1,i})^2\\ + (\hat{y}^t_{k|k-1} - \hat{y}^s_{k|k-1,i})^2\},\end{aligned} \tag{18}$$

subjected to $\sum_{i=1}^{n_s} S_i = n$, where n_s and n are the number of total and selected sensors respectively. $\hat{x}_{k|k-1}$ is the predicted x position of target at time k.

2) FIM-BASED COST FUNCTION

The FIM is a mathematical tool used in statistics to quantify the amount of information that an observable random variable $\mathcal{Y}$ contains about an unknown parameter X. It is defined as the negative of the expected value of the Hessian of the log-likelihood function with respect to X:

$$FIM = -E\left[\nabla^2_X\{\log L(X)\}\right],$$

where $L(X) = p(\mathcal{Y}|X)$ is the likelihood function of the observed data given the parameter X, and $E[.]$ denotes the expected value. In simpler terms, the FIM measures how sensitive the likelihood function is w.r.t the variation of X. It is a symmetric, positive definite matrix that contains information about the covariance of the estimators.

Let J_k represents the FIM, and is defined by the relation [36]

$$P_{k|k} \triangleq \mathbb{E}[(\hat{X}^t_k - X^t_k)(\hat{X}^t_k - X^t_k)^\tau] \geq J^{-1}_k, \tag{19}$$

where $\hat{X}^t_k$ and $P_{k|k}$ are the estimated state of the target and corresponding error covariance matrix. The value of J^{-1}_k is the posterior Cramer-Rao lower bound (PCRLB) matrix, always less or equal to $P_{k|k}$. FIM is initialized by the inverse of an initial error covariance matrix, and its initialization will be discussed in the simulation. The value of FIM at the current instant is calculated recursively from its previous instant by combining with the current information gained by the sensors, *i.e.*

$$J_k = J_{X^t_k} + J_{\mathcal{Y}_k}, \tag{20}$$

where $J_{X^t_k}$ is the predicted information of the target received from the previous FIM and $J_{\mathcal{Y}_k}$ represents the measurement information matrix at time instant k. Under the assumption that the measurement of sensors is mutually independent, the total information available at tracker $J_{\mathcal{Y}_k}$ is calculated as the sum of all the selected sensors measurement information, *i.e.*

$$J_{\mathcal{Y}_k} = \sum_{i=1}^{n} J_{\mathcal{Y}_{k,i}}. \tag{21}$$

FIM calculation is presented in [21], and it can be calculated recursively by

$$J_k = \underbrace{\mathcal{D}^{22}_k - \mathcal{D}^{21}_k[J_{k-1} + \mathcal{D}^{11}_k]^{-1}\mathcal{D}^{12}_k}_{J_{X^t_k}} + J_{\mathcal{Y}_k}, \tag{22}$$

where

$$\begin{aligned}\mathcal{D}^{11}_k &= \mathbb{E}\{-\Delta^{k-1}_{k-1} \ln p(X^t_k|X^t_{k-1})\},\\ \mathcal{D}^{12}_k &= \mathbb{E}\{-\Delta^{k-1}_{k} \ln p(X^t_k|X^t_{k-1})\},\\ \mathcal{D}^{21}_k &= (\mathcal{D}^{12}_k)^\tau,\\ \mathcal{D}^{22}_k &= \mathbb{E}\{-\Delta^{k}_{k} \ln p(X^t_k|X^t_{k-1})\},\\ J_{\mathcal{Y}_k} &= \mathbb{E}\{-\Delta^{k-1}_{k} \ln p(\mathcal{Y}_k|X^t_k)\},\end{aligned}$$

and p is used to represent the probability density function (pdf), and Δ is a second order partial derivative operator.

For a system that consists of a nonlinear process and measurement, the values of $\mathcal{D}^{11}_k$, $\mathcal{D}^{12}_k$, $\mathcal{D}^{21}_k$, $\tilde{\mathcal{D}}^{22}_k$ and $J_{\mathcal{Y}_k}$ are given by [36]

$$\begin{aligned}\mathcal{D}^{11}_k &= F^\tau Q^{t\;-1}_k F,\\ \mathcal{D}^{12}_k &= -F^\tau Q^{t\;-1}_k,\\ \mathcal{D}^{21}_k &= (\mathcal{D}^{12}_k)^\tau,\\ \tilde{\mathcal{D}}^{22}_k &= Q^{t\;-1}_k,\\ J_{\mathcal{Y}_k} &= \sum_{i=1}^{n} \mathbb{E}[J_{\mathcal{Y}_{k,i}}] = \sum_{i=1}^{n} \mathbb{E}[H^{t^\tau}_{k,i}\hat{R}^{-1}_{k,i}H^t_{k,i}],\end{aligned}$$

where F is a Jacobian matrix of process function, $H^t_{k,i} = \nabla_{X^t_k} h(X^t_k, X^s_{k,i})|_{X^t_k=\hat{X}^t_{k|k-1}}$ is the Jacobian matrix of $i-$ th sensor's measurement, and $\hat{R}_{k,i}$ is the Taylor series based equivalent measurement noise covariance matrix as given in (11).

The FIM based cost function can be formed by following two different ways:

(i) *Method 1 (FIM-1)* : The FIM only at an instant of selection is used to define the cost function. An optimal sensor set S_k^* is given by [13]

$$S_k^* = \arg\min_{S_i} \operatorname{trace}\left\{\left[J_{X_k^t} + \sum_{i=1}^{n_s} S_i J_{\mathcal{Y}_{k,i}}\right]^{-1}\right\}, \tag{23}$$

subjected to $\sum_{i=1}^{n_s} S_i = n$.

(ii) *Method 2 (FIM-2)* : If we want to select the sensors at an interval that is more than the sampling time, all past measurement information received in that interval should be considered, which is not the case in the above cost function. To overcome it, the following cost function (FIM-2) is presented which considers the FIM at each time step until the next selection of the sensors happens [13]:

$$S_k^* = \arg\min_{S_i} \sum_{\tau=k}^{k+l-1} \operatorname{trace}\left\{\left[J_{X_\tau^t} + \sum_{i=1}^{n_s} S_i J_{\mathcal{Y}_{\tau,i}}\right]^{-1}\right\}, \tag{24}$$

subjected to $\sum_{i=1}^{n_s} S_i = n$, where T_s is the sensor selection interval, and $l = T_s/T$.

B. OPTIMIZATION OF THE COST FUNCTIONS

All the three cost functions (18), (23) and (24) are minimized using direct search method. For a small number of total engaged sensors (n_s) and selected sensors (n), a combinatorial optimization [37] is best suited as a search algorithm. This method generates all the possible sensor combinations, and the function is compared to find the active sensor set. This method is not useful for large values of n_s and n because the total number of possible combinations will be ${}^{n_s}C_n$, and it becomes time and memory-consuming due to large possible combinations. So, the selection-based local search method is developed as an alternative to find the optimum solution, and we used it here to optimize the cost function. The algorithm of the local search method is presented in the Algorithm 1.

Algorithm 1 Local Search Method [37]

```
[$S_k^*$, $\mathcal{Y}_k$] = Local_Search(obj, $n$, $n_s$)
- Initialize the universal sensor set
  $U = \{1, 2, \cdots, n_s\}$,
- Initially put all the sensors in passive mode
  $S_k^* = 0_{1\times n}$, and $\mathcal{Y}_k = [\,]$.
- Initialize the optimal sensor set
  $C_s = U_{1:n}$, $U = U - C_s$.
for $i = 1 : n$
  for $j = 1 : n_s - n$
      - Generate the immediate neighbor point by:
          $N_s = C_s, N_{s_i} = U_j$
        if obj($N_s$) < obj($C_s$)
      - Update the $j$-th value of $U$ by:
        $U_j = C_{s_i}$, and $C_s = N_s$.
        else
          - $C_s$ holds the previous value
        end if
  end for
  - Update the $S_k^*$ and $Y_k$ by
   $S_k^*(C_{s_i}) = 1$, $\mathcal{Y}_k = [\mathcal{Y}_k;\ \mathcal{Y}_{k,C_{s_i}}]$.
end for
```

V. SENSOR SELECTION AND TRACKING CO-DESIGN

A. SRF WITH NONLINEAR PROCESS

Traditional SRF deals with linear process equations. So, in a scenario when the process equation becomes nonlinear, we need to modify the SRF so that a nonlinear system with bearing measurements can be tracked. To deal with nonlinear target dynamics, deterministic sample points are generated from posterior pdf. The process update is done on the deterministic sample points and updated mean and error covariance are calculated. Those prior mean and covariance are used in shifted Rayleigh measurement update. We may call this algorithm as deterministic sample point-based SRF (DS-SRF).

Prior to conducting a measurement update of a target, it is necessary to estimate the sensor state perfectly and to calculate an equivalent measurement covariance. It is already mentioned that the tracker possesses initial position information for all sensors with some uncertainty and each sensor state model is linear and Gaussian, so it is possible to obtain both the predictive state and its corresponding covariance by

$$\hat{X}^s_{k|k-1,i} = F\hat{X}^s_{k-1|k-1,i}, \tag{25}$$

$$P^s_{k|k-1,i} = FP^s_{k-1|k-1,i}F^\tau + Q^s_{k,i}. \tag{26}$$

In addition to the bearing angles of all sensors, the tracker also possesses bearing angle information of all sensors w.r.t its own location. By incorporating this information along with the aforementioned sensor bearing angles into a deterministic sample points based approach, the tracker can obtain a posterior estimate and corresponding covariance $(\hat{X}^s_{k|k,i}, P^s_{k|k,i})$ for each sensor. To perform the measurement update of the target, a projection of sensor measurement is made on a unit circle, given by

$$b_{k,i} = [\sin\mathcal{Y}_{k,i},\ \cos\mathcal{Y}_{k,i}]^\tau. \tag{27}$$

The shifted Rayleigh variable $\mathtt{z}_k$ is computed as

$$\mathtt{z}_k = [b_{k,i}{}^\tau V_k^{-1} b_{k,i}]^{-1/2} b_{k,i}{}^\tau V_k^{-1}[H\hat{X}_{k|k-1,i}], \tag{28}$$

where $\hat{X}_{k|k-1,i}$ is predictive relative state vector from target to sensor *i.e.* $\hat{X}_{k|k-1,i} = \hat{X}^t_{k|k-1} - \hat{X}^s_{k|k-1,i}$, and $V_k = HP^t_{k|k-1}H^\tau + \hat{R}_{k,i}$. The mean, ζ_k and covariance, δ_k of $\mathtt{z}_k$

is computed by

$$\zeta_k = [b_{k,i}{}^{\tau} V_k^{-1} b_{k,i}]^{-1/2} \rho(\mathrm{z}_k), \tag{29}$$

$$\delta_k = [b_{k,i}{}^{\tau} V_k^{-1} b_{k,i}]^{-1} (2 + \mathrm{z}_k \rho(\mathrm{z}_k) - \rho^2(\mathrm{z}_k)), \tag{30}$$

where constants $\rho(\mathrm{z}_k)$, is given by

$$\rho(\mathrm{z}_k) = \frac{\mathrm{z}_k e^{-\mathrm{z}_k^2/2} + \sqrt{2\pi}(\mathrm{z}_k^2 + 1)\mathbb{F}(\mathrm{z}_k)}{e^{-\mathrm{z}_k^2/2} + \sqrt{2\pi}\,\mathrm{z}_k \mathbb{F}(\mathrm{z}_k)}, \tag{31}$$

where $\mathbb{F}(\mathrm{z}_k)$ is the cumulative distribution function of a standard normal variable. The Kalman gain of the filter is calculated by

$$K_k = P^t_{k|k-1} H^{\tau} V_k{}^{-1}. \tag{32}$$

The posterior mean and covariance are computed by

$$\hat{X}_{k|k,i} = \hat{X}_{k|k-1,i} + K_k[\zeta_k b_{k,i} - H\hat{X}_{k|k-1,i}], \tag{33}$$

$$P^t_{k|k} = (\mathrm{I} - K_k H) P^t_{k|k-1} + \delta_k K_k b_{k,i} b_{k,i}{}^{\tau} K_k{}^{\tau}, \tag{34}$$

and

$$\hat{X}^t_{k|k} = \hat{X}_{k|k,i} + \hat{X}^s_{k|k,i}. \tag{35}$$

B. CO-DESIGN

Now, sensor selection and tracking filters should run together. The prior estimate from the tracking filter is used in the sensor selection problem and once sensors are selected, their measurements are used to estimate the states of the target. A complete algorithm of sensor selection and tracking with the DS-SRF is presented in the Algorithm 2. We also implemented popular deterministic sample points filters such as the CKF, the UKF, the CQKF, and the GHF along with the sensors selection algorithms. A detailed comparison of such results is provided in the next section.

VI. SIMULATION RESULTS

In this work, we choose a D-shaped surveillance area which is a combination of a rectangle and a semicircle as shown in Fig. 1. Let the area of the rectangle is A_r and that of the semicircular is A_s. Suppose we have to generate a total N number of uniformly distributed samples in our surveillance region. The selection probability of each part is calculated by

$$\begin{bmatrix} p_r \\ p_s \end{bmatrix} = \frac{1}{(A_r + A_s)} \begin{bmatrix} A_r \\ A_s \end{bmatrix}. \tag{36}$$

First, we generate the n_r number of random samples inside the rectangle (Let the set is denoted by $\mathcal{Q}^r$) and n_s number of samples in a semicircle (Let the set is $\mathcal{Q}^s$). Concatenating the samples n_r and n_s ($n_r + n_s = N$), the total number of uniformly distributed sample points *i.e.* $\mathcal{Q} = [\mathcal{Q}^r\ \mathcal{Q}^s]$ obtained. For a detailed discussion about uniformly distributed random number generation in any arbitrary region, please see Appendix A. In this section, we consider two engagement scenarios: (i) a target moving in a straight line with a nearly constant velocity (ii) a target maneuvering with a constant but unknown turn rate. The results of tracking along with sensor selection are presented in this section.

Algorithm 2 Pseudo-Code for Sensor Selection and Tracking With DS-SRF

```
• Initialization
    – Initialize the filter with $\hat{X}^t_{0|0}$ from (37), and $\hat{X}^s_{0|0,i} \sim \mathcal{N}(X^s_{0,i}, P^s_{0|0,i}),\ i = 1, \cdots, n_s$.
• Time update for target
    – Generate support points $\hat{\mathcal{X}}^t_{k-1|k-1,j}$ from $\hat{X}^t_{k-1|k-1}$, and $P^t_{k-1|k-1}$.
    – Update the mean:
          $$\hat{X}^t_{k|k-1} = \sum_{j=1}^{n_p} W_j f(\hat{\mathcal{X}}^t_{k-1|k-1,j}).$$
    – Update the error covariance:
          $$P^t_{k|k-1} = \sum_{j=1}^{n_p} W_j (f(\hat{\mathcal{X}}^t_{k-1|k-1,j}) - \hat{X}^t_{k|k-1}) (f(\hat{\mathcal{X}}^t_{k-1|k-1,j}) - \hat{X}^t_{k|k-1})^{\tau} + Q^t_k.$$
• Update for sensors:
          $$\hat{X}^s_{k|k,i} = \hat{X}^s_{k|k-1,i} = F\hat{X}^s_{k-1|k-1,i},$$
          $$P^s_{k|k,i} = P^s_{k|k-1,i} = FP^s_{k-1|k-1,i}F^{\tau} + Q^s_{k,i}.$$
• Sensor selection
    – Calculate cost function and select sensor set.
• Measurement update for target
  for $(i = 1 : n_s) \&\& (S^*_k(i) == 1)$
    – Calculate overall measurement noise covariance $\hat{R}_{k,i}$, using (13).
    – Obtain posterior estimate and error covariance by (27)-(34).
  end
```

A. TRACKING FILTER INITIALIZATION

The target's position is initialized using triangulation of two bearing angles received from two measurement sensors. Target velocity is initialized from two successive positions. So, at 0−th instance, the x position and y position are given as

$$x^t_0 = (x^s_{0,2} \tan \mathcal{Y}_{0,1} - x^s_{0,1} \tan \mathcal{Y}_{0,2} + (y^s_{0,1} - y^s_{0,2}) \tan \mathcal{Y}_{0,1} \tan \mathcal{Y}_{0,2})/(\tan \mathcal{Y}_{0,1} - \tan \mathcal{Y}_{0,2}),$$

and

$$y^t_0 = x^s_{0,2} - x^s_{0,1} + y^s_{0,1} \tan \mathcal{Y}_{0,1} - y^s_{0,2} \tan \mathcal{Y}_{0,2})/(\tan \mathcal{Y}_{0,1} - \tan \mathcal{Y}_{0,2}),$$

where $\mathcal{Y}_{0,1}$ represents the measurement at 0-th step obtained from 1st sensor. Similarly x^t_1 and y^t_1 are calculated and the state vector is initialized as

$$\hat{X}^t_{0|0} = [x^t_0,\ \frac{x^t_1 - x^t_0}{T},\ y^t_0,\ \frac{y^t_1 - y^t_0}{T}]^{\tau}. \tag{37}$$

TABLE 1. Tracking parameters.

Parameters	Scenario-1	Scenario-2
No. of operational sensors (n_s)	100	100
No. of selected sensors (n)	2, 3, 4	2, 3, 4
Measurement sampling interval (T)	0.5 min	0.5 min
Sensor selection interval (T_s)	3 min	3 min
Process noise intensities $(\bar{q}_1, \bar{q}_2)$	1.944 m^2/min^3	0.01 rad^2/min^3
measurement noise cov (σ_θ^2)	4°	4°
Initial target location	$(12.5, 8.5)$Km	$(13.5, 9.5)$Km
Target speed	10 Knots	10 Knots
Target initial coarse angle	$-120°$	$-165°$
Uncertainty in sensor position (σ_p)	10 m	10 m
Turn rate (ω)	–	1.84°/min

To calculate the initial error covariance, we consider an augmented vector $\mathcal{V} = [x^s_{0,1}\ y^s_{0,1}\ x^s_{0,2}\ y^s_{0,2}\ \mathcal{Y}_{0,1}\ \mathcal{Y}_{0,2}]^\tau$. Next, we calculate the Jacobian of the initial target state vector as $\mathcal{H} = \nabla_{\mathcal{V}} \hat{X}^t_{0|0}$, and initialize the sensor error covariance by $P^s_{0|0,i} = \text{diag}([\sigma_p^2,\ \sigma_v^2,\ \sigma_p^2,\ \sigma_v^2])$. The error covariance of $\mathcal{V}$ is given by $P_{\mathcal{V}\mathcal{V}} = \text{diag}([HP^s_{0|0,1}H^\tau,\ HP^s_{0|0,2}H^\tau,\ R_{0,1},\ R_{0,2}])$. The error covariance of the target state is initialized by $P^t_{0|0} = \mathcal{H}P_{\mathcal{V}\mathcal{V}}\mathcal{H}^\tau$.

B. SIMULATION RESULTS OF SCENARIO-1

In scenario-1, we consider a target moving in a straight line with a nearly constant velocity. In this case, the target is represented with the model as described in (1). The target starts from a location of (12.5, 8.5) km and moves towards the southwest with a velocity of 10 knots and at a coarse angle of −120° with respect to the true north. The simulation parameters are taken from [13] and [31] and are listed in Table 1. The sensors are uniformly distributed in the surveillance region and are drifting due to sea currents as shown in Fig. 1. Sensors are selected at every T_s minute, where during the simulation T_s is taken as 1, 3, 6, and 9 minutes. It means that the tracker receives a total $(L = \frac{T_s}{T})$ number of measurement samples in a single sensor selection interval. Several deterministic sample point filters such as the CKF, UKF, CQKF, GHF, and SRF are applied along with the sensor selection algorithm which selects a user-defined number of sensors at each interval. The estimator uses the measurements received by the selected sensor to track the target. Selected sensors obtained from ED, FIM-1 and FIM-2 cost functions (for $T_s = 3$, $\sigma_p = 10$) at any arbitrary $k = 36$, are shown in Fig. 1. In this figure, black dots are the sensors' initial positions, and sensors' drifts are shown using black dotted lines.

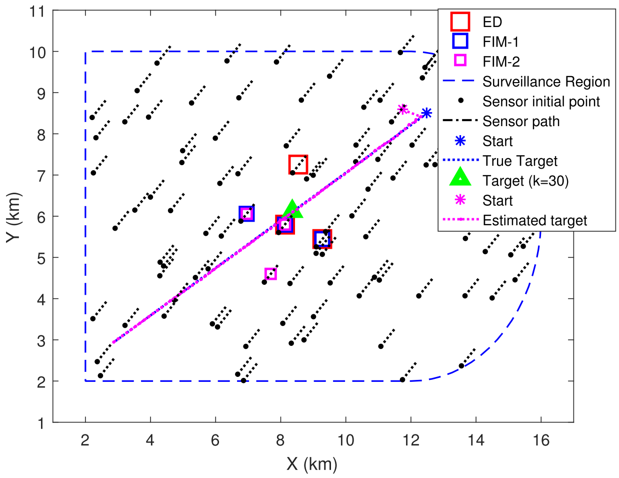

FIGURE 1. Tracking scenario-1: target and sensor trajectories along with selected sensors at an instant $k = 36$, when the target moves with a near constant velocity.

Cramer-Rao lower bound (CRLB) is initialized by the initial state error covariance matrix defined earlier in this section. The CRLBs are computed for $T_s = 3$, $\sigma_p = 10$, with 2 and 4 sensors and for different selection methods and they are plotted in Fig.2 and 3. The figures show that FIM-2

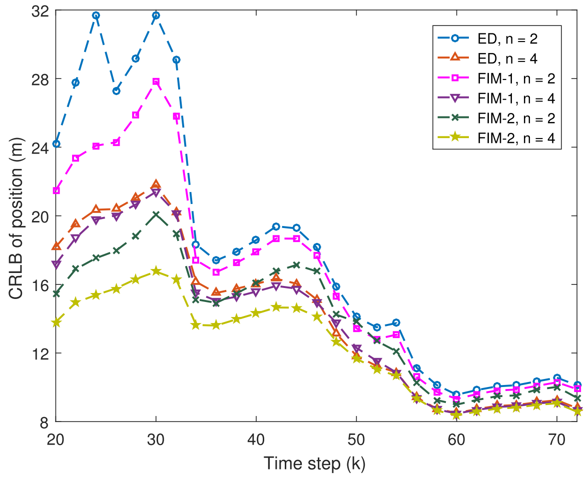

FIGURE 2. CRLB of position (for $T_s = 3$, $\sigma_p = 10$) using different sensor selection methods and varying the number of selected sensors when target moves with a constant velocity (scenario-1).

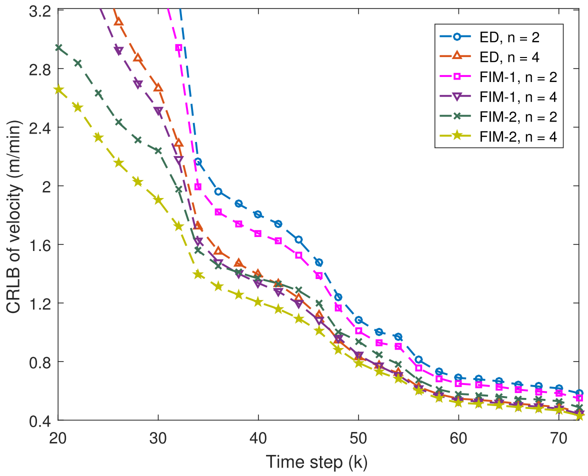

FIGURE 3. CRLB of velocity (for $T_s = 3$, $\sigma_p = 10$) using different sensor selection methods and varying the number of selected sensors when target moves with a constant velocity (scenario-1).

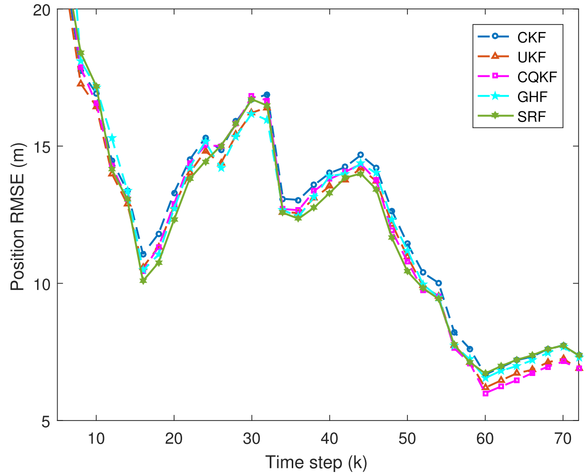

FIGURE 4. RMSE of position (for $T_s = 3$, $n = 3$, $\sigma_p = 10$) by using different filtering techniques with FIM-2 based sensor selection for a target moving in a near constant velocity (scenario-1).

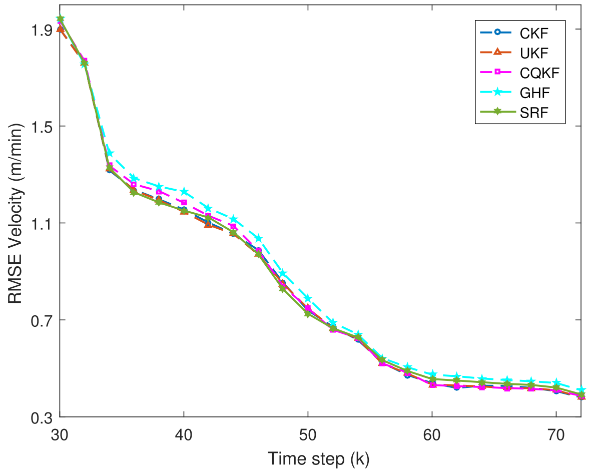

FIGURE 5. RMSE of velocity (for $T_s = 3$, $n = 3$, $\sigma_p = 10$) by using different filtering techniques with FIM-2 based sensor selection for a target moving in a near constant velocity (scenario-1).

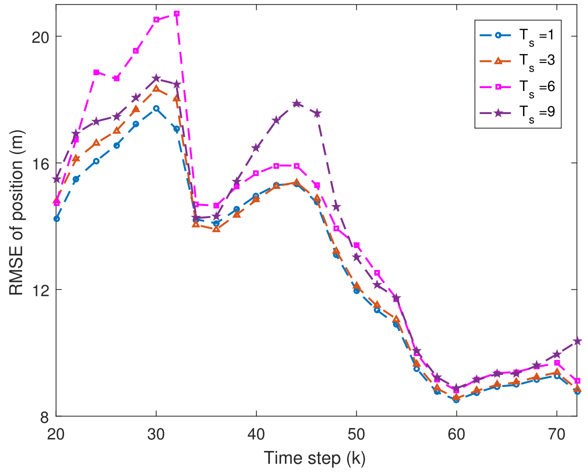

FIGURE 6. RMSE of position using SRF (for $\sigma_p = 10$, $n = 3$) for different sensor selection interval (T_s in minute) using FIM-2 based sensor selection for a target moving in a near constant velocity (scenario-1).

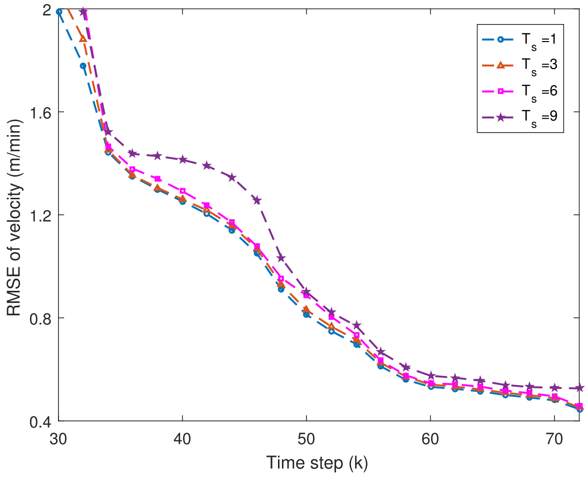

FIGURE 7. RMSE of velocity using SRF (for $\sigma_p = 10$, $n = 3$) for different sensor selection interval (T_s in minute) using FIM-2 based sensor selection for a target moving in a near constant velocity (scenario-1).

based selection provides the lowest and most smooth CRLB of both position and velocity among all three methods. It can also be seen that more the number of selected sensors lower be the CRLB.

We have experimented with several noise covariances in the range of $(1°)^2$ to $(7°)^2$ and tested in the designed algorithm. It is found that by increasing the noise covariance, the Cramer- Rao bound shifts up, and a slight increase in the track divergences occurs during tracking.

The filters are initialized as described at the beginning of this section. The SRF is implemented along with sensor selection as given in Algorithm 2. Similar algorithms are implemented for deterministic sample point filters. Root mean square error (RMSE) of position and velocity of the target for $T_s = 3$, $\sigma_p = 10$, $n = 3$, with FIM-2 based sensor selection, obtained from different filters are compared in Fig. 4 and Fig. 5. Note that RMSEs in figures are calculated out of 1000 Monte Carlo runs and by excluding the track lost cases. From the figures, it is found that the RMSEs of all the filters are comparable to each other.

The RMSE of SRF for $\sigma_p = 10$, $n = 3$, FIM-2 based selection for different sensor selection intervals ($T_s = 1, 3, 6, 9$ minutes) are plotted in Fig. 6 and Fig. 7. From the figures, it can be seen that the lower be the selection interval, the smaller be the RMSE of position and velocity. The RMSE of SRF for $T_s = 3$, $n = 3$, FIM-2 based selection are plotted for various sensor location uncertainties ($\sigma_p = 0, 10, 25, 50$) in Fig. 8 and Fig. 9. From the figure, it is observed that with the increase in the sensor location uncertainty, the accuracy of the estimation decreases.

It has been observed that sometimes the estimators fail to track the target. A track is said to diverge if the final estimation error in position is greater than some threshold, e_b. Throughout the simulation, we took the value of e_b as

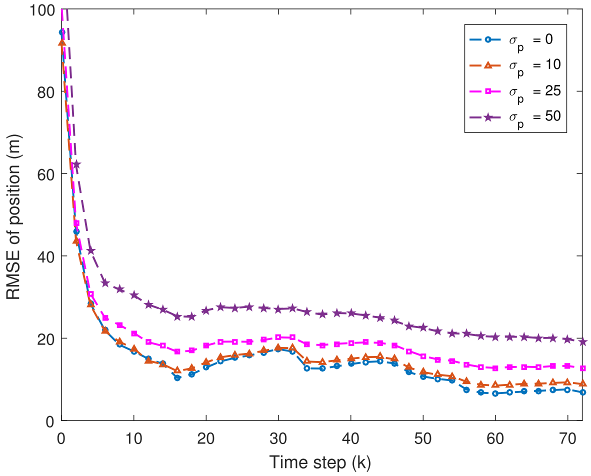

FIGURE 8. RMSE of position using SRF (for $T_s = 3, n = 3$) by varying sensor position uncertainty in scenario-1.

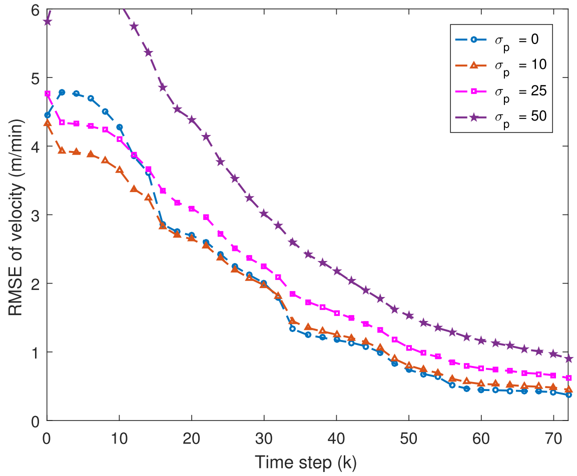

FIGURE 9. RMSE of velocity using SRF (for $T_s = 3, n = 3$) by varying sensor position uncertainty in scenario-1.

50 meters. We tabulated the percentage of track divergence calculated out of 1000 Monte Carlo runs for various filters by varying the sensor selection method, the number of the selected sensors (n), and sensor position uncertainty in Table 2. From the table, it is observed that the FIM-2 provides the lowest track divergence. Among the filters, the performance of the SRF is the best and it provides almost zero percent track divergence. Also, we note that with the increase in the number of selected sensor percentage of track divergence slightly decreases, and with the increase of sensor location uncertainty it increases rapidly.

The relative computational time of all filters for various selection methods and varying the sensor selection interval are listed in Table 3. From the table, it can be seen that the computation times of all the filters are comparable. However, they increase when we select more number of sensors, and they decrease with the increase in sensor selection interval time. Further the reader may also note that FIM-based selection methods take more than double the time to execute, compared to ED-based selection method.

To check the consistency of the proposed filter, averaged normalized estimation error squared (ANEES) is calculated

TABLE 2. Percentage of track loss for various sensor selection methods, tracking filters, and sensor position uncertainty.

Selection method	No. of Sensors	Sensor position uncertainty	Scenario-1					Scenario-2				
			CKF	UKF	CQKF	GHF	SRF	CKF	UKF	CQKF	GHF	SRF
ED	$n = 2$	$\sigma_p = 0$	2.7	2.4	2.5	2.6	0	4.3	4.7	4.4	4.3	0.2
		$\sigma_p = 10$	3.1	3.0	2.9	2.9	0	4.8	4.7	4.7	4.6	0.2
		$\sigma_p = 25$	4.3	4.2	4.2	4.1	0	5.2	5.2	5.1	5.1	0.3
		$\sigma_p = 50$	17.1	15.2	16.7	17.3	0.3	16.0	15.5	15.7	15.2	0.5
	$n = 4$	$\sigma_p = 0$	2.4	1.9	2.4	2.3	0	3.7	3.8	3.7	3.5	0.1
		$\sigma_p = 10$	3.2	3.5	3.5	2.9	0	3.9	3.9	3.7	3.5	0.1
		$\sigma_p = 25$	4.7	4.6	4.7	4.2	0	4.3	4.2	4.3	4.1	0.2
		$\sigma_p = 50$	13.1	13.2	14.1	13.9	0.2	13.7	13.9	13.9	13.6	0.2
FIM-1	$n = 2$	$\sigma_p = 0$	2.6	2.4	2.4	2.5	0	3.8	3.9	3.8	3.6	0.2
		$\sigma_p = 10$	3.2	3.4	3.3	3.1	0	4.1	4.3	4.3	3.9	0.1
		$\sigma_p = 25$	5.0	4.9	4.7	5.1	0	4.9	5.1	5.2	4.8	0.3
		$\sigma_p = 50$	16.3	15.3	15.8	17.0	0.3	14.6	14.9	14.7	14.5	0.4
	$n = 4$	$\sigma_p = 0$	2.3	2.4	2.3	2.4	0	3.3	3.4	3.3	3.3	0
		$\sigma_p = 10$	3.1	3.6	3.4	3.2	0	3.6	3.7	3.7	3.5	0.1
		$\sigma_p = 25$	4.2	4.5	4.3	4.6	0	4.3	4.1	3.9	4.0	0.2
		$\sigma_p = 50$	12.3	11.9	13.2	13.7	0.2	12.8	12.9	12.9	12.6	0.3
FIM-2	$n = 2$	$\sigma_p = 0$	2.1	1.9	1.9	2.1	0	3.6	3.7	3.7	3.5	0
		$\sigma_p = 10$	3.0	2.9	2.9	3.0	0	3.9	3.9	3.8	3.6	0.1
		$\sigma_p = 25$	4.8	4.8	4.7	4.5	0	4.4	4.5	4.4	4.4	0.2
		$\sigma_p = 50$	12.1	13.2	13.7	13.3	0.2	14.2	14.4	15.1	14.4	0.2
	$n = 4$	$\sigma_p = 0$	1.5	1.3	1.4	1.3	0	3.2	3.1	3.1	3.0	0
		$\sigma_p = 10$	2.2	2.1	2.2	2.0	0	3.4	3.3	3.4	3.2	0
		$\sigma_p = 25$	3.1	3.0	2.9	3.0	0	3.9	4.1	3.9	3.7	0.1
		$\sigma_p = 50$	12.2	12.0	11.8	11.7	0.1	11.8	11.1	11.9	11.8	0.1

TABLE 3. Relative computational time for various sensor selection methods, tracking filters, and sensor selection interval.

Selection method	No. of sensors	Selection interval	CKF	UKF	CQKF	GHF	SRF
ED	$n = 2$	$T_s = 1$	1	1.0094	0.9813	1.002	0.974
		$T_s = 3$	0.5393	0.5138	0.5175	0.531	0.5258
		$T_s = 6$	0.4176	0.4022	0.4037	0.4266	0.4097
		$T_s = 9$	0.4731	0.3678	0.3645	0.3840	0.3708
	$n = 4$	$T_s = 1$	1.6736	1.617	1.6365	1.6676	1.6593
		$T_s = 3$	0.785	0.8440	0.7610	0.786	0.7657
		$T_s = 6$	0.5618	0.5440	0.5388	0.6018	0.5546
		$T_s = 9$	0.4916	0.4759	0.4710	0.4998	0.4782
FIM-1	$n = 2$	$T_s = 1$	2.5885	2.5690	2.5634	2.6404	2.5621
		$T_s = 3$	1.0948	1.0905	1.5709	1.0957	1.0939
		$T_s = 6$	0.7316	0.7077	0.7057	0.7237	0.7151
		$T_s = 9$	0.6116	0.5925	0.5918	0.6788	0.5997
	$n = 4$	$T_s = 1$	4.8175	4.7372	4.7015	4.7341	4.6791
		$T_s = 3$	1.8504	1.816	1.8261	1.8545	1.8435
		$T_s = 6$	1.1289	1.1064	1.0978	1.1337	1.1408
		$T_s = 9$	0.8900	0.9472	0.8581	0.9018	0.8787
FIM-2	$n = 2$	$T_s = 1$	2.6949	2.6766	2.6476	2.6687	2.6425
		$T_s = 3$	1.1739	1.1492	1.1508	1.1641	1.1577
		$T_s = 6$	0.7947	0.7766	0.7795	0.7898	0.7792
		$T_s = 9$	0.6780	0.6546	0.6542	0.6684	0.6563
	$n = 4$	$T_s = 1$	4.9036	4.8569	4.9117	4.8412	4.8532
		$T_s = 3$	2.0111	1.9256	1.9085	1.9461	1.9140
		$T_s = 6$	1.1960	1.1747	1.1653	1.2079	1.1922
		$T_s = 9$	0.9527	0.9360	0.9309	0.9566	0.9292

by using the formula [31]

$$\text{ANEES} = \frac{1}{M_c}\sum_{j=1}^{M_c}(X_{k,j} - \hat{X}_{k|k,j})' P^{-1}_{k|k,j}(X_{k,j} - \hat{X}_{k|k,j}), \quad (38)$$

where M_c is the number of Monte-Carlo simulations respectively. A filter is considered as consistent if the ANEES lies between the lower bound (l_b) and upper bound (u_b) region *i.e.* ANEES $\in [l_b, u_b]$. When the ANEES is less than l_b, it indicates that the estimated posterior error covariance is very high as compared to the true value. Hence the filter is said to be under confident. Similarly, if the ANEES is more than u_b, it denotes that the estimated posterior error covariance is very small as compared to its true value. In such case, the filter is marked to be over confident. ANEES is the parameter to determine whether the filter is credible or not in the sense of self assessment. According to the small probability event principle [38], an estimator is not credible if an event having very small probability occurs on a single trial. This is possible when the ANEES is outside the region of very high probability (say, 95 %). For 95 % probability region, the lower bound (l_b) and the upper bound (u_b) can be calculated as

$$l_b = n_x[(1 - \frac{2}{9n_xM_c}) - 1.96\sqrt{\frac{2}{9n_xM_c}}]^3, \quad (39)$$

and

$$u_b = n_x[(1 - \frac{2}{9n_xM_c}) + 1.96\sqrt{\frac{2}{9n_xM_c}}]^3, \quad (40)$$

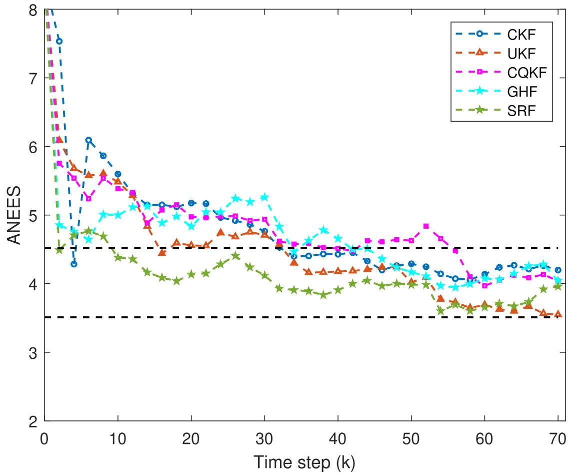

FIGURE 10. ANEES for various estimators (for $n = 3$, $T_s = 3$, $\sigma_p = 10$) when the sensors are selected using FIM-2, for scenario 1.

where n_x is the total number of states and in our case $n_x = 4$. We have calculated ANEES over the 100 Monte-Carlo runs at each estimation step and plotted for $\sigma_p = 10$, $T_s = 3$, $n = 3$, FIM-2 based selection in Fig. 10. The plot shows that almost all the ANEESs reach within the 95 percent confidence region after the 35-th step, which results in all designed filters performing adequately over the tracking interval.

C. SIMULATION RESULTS OF SCENARIO-2

Scenario-2 contains a target that is maneuvering with a nearly constant turn rate. In this case, the target is represented with

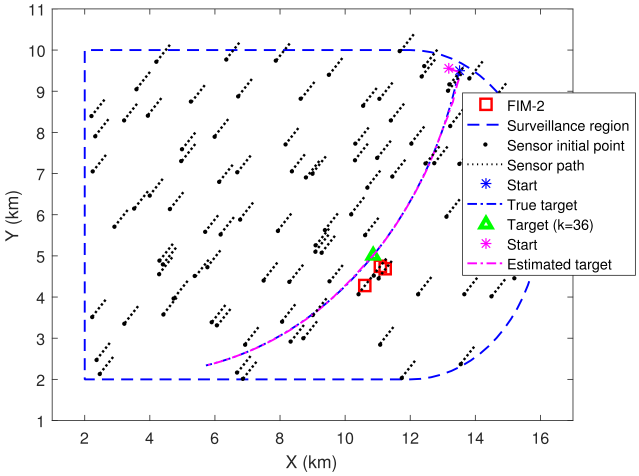

FIGURE 11. Tracking scenario-2: target and sensor trajectories along with selected sensors at an instant k = 36, when target moves with constant turn rate following a CT model.

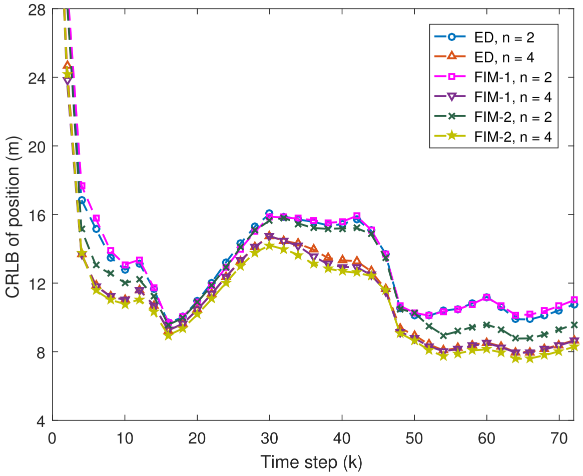

FIGURE 12. CRLB of position (for $T_s = 3$, $\sigma_p = 10$) when sensors are selected using ED, FIM-1, FIM-2 cost functions.

a coordinated turn (CT) model as we described in (4). The target starts from a location of $(13.5,\ \ 9.5)km$ and moves towards the southwest. The simulation parameters are listed in Table 1. At $k = 36$, sensor locations using FIM-2 cost function (for $T_s = 3, \sigma_p = 10$) are shown in Fig. 11.

Similar to scenario-1, the CRLB is computed for $T_s = 3$, $\sigma_p = 10$, in scenario-2 with 2 and 4 number of sensors which are selected using different cost functions. The CRLB results are plotted in Fig. 12 and Fig. 13. These plots show that FIM-2 based sensor selection provides the lowest CRLB among the all three methods. We note that with the increase in the number of sensors, the CRLB values decrease.

During estimation, the first four states are initialized in a similar way to scenario-1. The turn rate is initialized with a mean $1.84^\circ/min$ and covariance $1^{\circ 2}/min^2$. RMSE results obtained from various filters (when sensors are selected using FIM-2 method) are compared in Fig. 14 and Fig. 15. From the figures, it is found that the RMSEs of all the filters are comparable to each other.

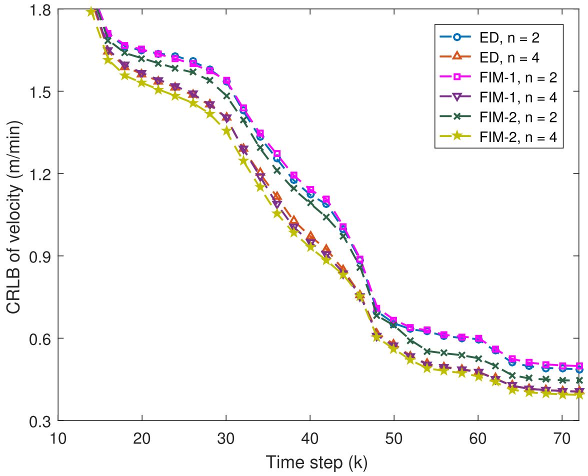

FIGURE 13. CRLB of velocity (for $T_s = 3$, $\sigma_p = 10$) when sensors are selected using ED, FIM-1, FIM-2 cost functions.

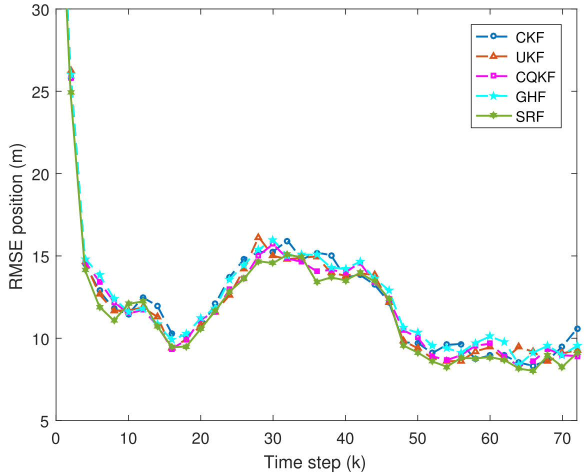

FIGURE 14. RMSE of positions (for $T_s = 3$, $n = 3$, $\sigma_p = 10$) obtained by using different filtering techniques with FIM-2 based sensor selection in scenario-2.

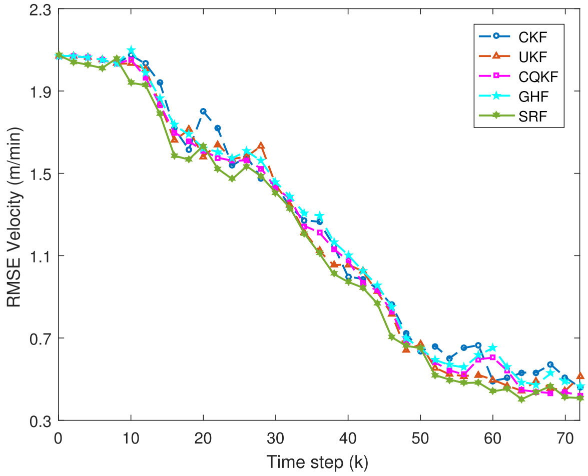

FIGURE 15. RMSE of velocity (for $T_s = 3$, $n = 3$, $\sigma_p = 10$) obtained by using different filtering techniques with FIM-2 based sensor selection in scenario-2.

The RMSEs of SRF for $T_s = 3$, $n = 3$, with FIM-2 based sensor selection are plotted for various sensor position uncertainties ($\sigma_p = 0, 10, 25, 50$) in Fig. 16, and Fig. 17.

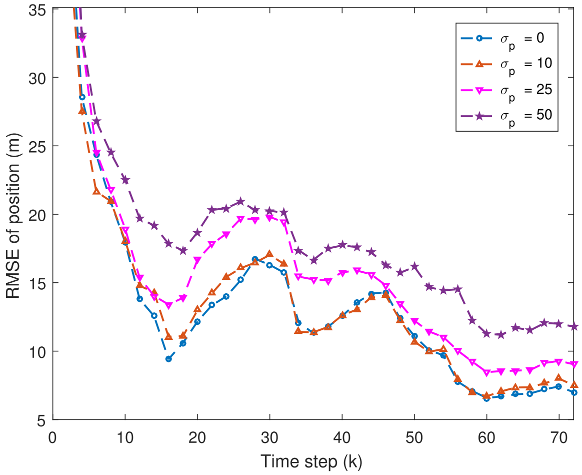

FIGURE 16. RMSE of position using SRF (for $T_s = 3, n = 3$) for various σ_p when FIM-2 is used for selecting sensors in scenario-2.

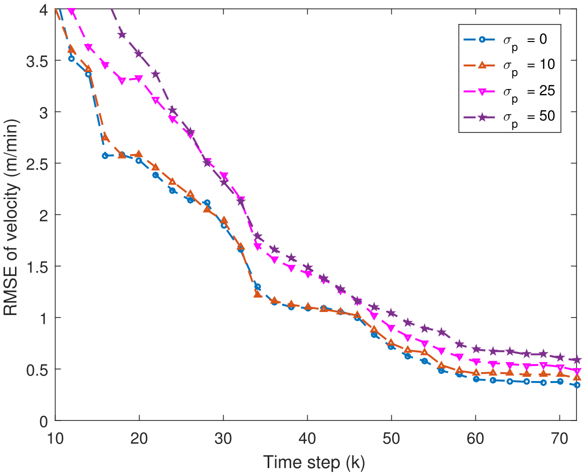

FIGURE 17. RMSE of velocity using SRF (for $T_s = 3, n = 3$) for various σ_p when FIM-2 is used for selecting sensors in scenario-2.

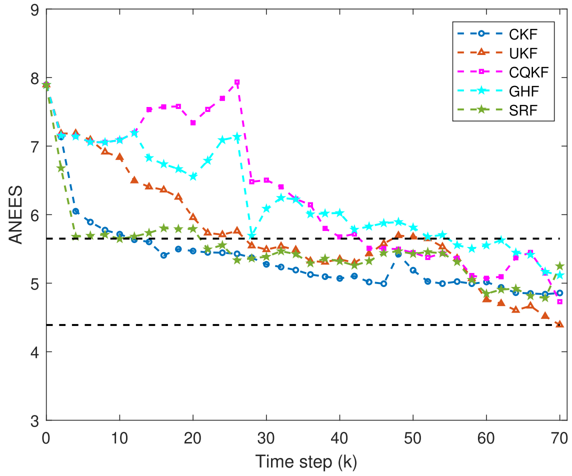

FIGURE 18. ANEES comparison (for $n = 3, T_s = 3, \sigma_p = 10$) when sensors are selected using FIM-2 in scenario-2.

From the figures, it is noted that with the increase in sensor location uncertainty, the accuracy of the estimation decreases.

The percentage of track loss for different sensor selection methods, number of selected sensors, and sensor position uncertainty are also tabulated in Table 2. The track loss condition is kept the same as described in scenario-1. From the table, it is observed that FIM-2 provides the lowest number of diverged tracks. Among the filters, the performance of the SRF is the best and it provides almost zero percent of track loss. With the increased number of selected sensor, percentage of track loss slightly decreases and with the increase of sensor location uncertainty it increases rapidly.

The ANEES results for $\sigma_p = 10$, $T_s = 3$, $n = 3$, with FIM-2 based selection are plotted in Fig. 18. From the plot, it is found that ANEESs of almost all the filters reach within the 95 percent confidence region after 50-th step of the run.

VII. CONCLUSION AND FUTURE WORK

The paper co-designs tracking and sensor selection to localize an underwater target using multiple passive sonars, deployed uniformly over the sea surface of arbitrary contour. The proposed tracking algorithm is capable of selecting a few sensors and it tracks the target using the measurements of those selected sensors in presence of sensor location uncertainty, and drift due to sea current. The sensor selection algorithm uses the FIM-based cost functions and for tracking various Gaussian filters and the SRF are designed. The co-design of the SRF and FIM-based sensor selection method provides better performance in terms of RMSE and percentage of track divergence compared to other Gaussian filters. The present work is being extended for a decentralized tracking scenario which would be useful to track a target in a very large surveillance area.

APPENDIX A
GENERATION OF POINTS, UNIFORMLY DISTRIBUTED IN THE SURVEILLANCE REGION

Linear congruential generator (LCG) [39] which generates a uniform random number in between 0 and 1 is a very popular and most preferable deterministic approach to obtain independent identically distributed (iid) samples. Amongst n iid samples, it is assumed that $\mathcal{Q}_i$ is the i^{th} sample of the random sequence, and is given by $\mathcal{Q}_i = x_i/m$, where x_i is calculated recursively as

$$x_i = mod(ax_{i-1} + c, m), \quad i = 1, \cdots, n. \tag{41}$$

Here, mod is a modulo operator which returns the remainder after the division of $ax_{i-1}+c$ by m. The parameters a, m, and c are known as multiplier, modulus, and increment respectively and their ranges are as follows: (i) $m > 0$ (ii) $m < a > 0$ (iii) $0 \leq c < m$.The value of m is generally chosen to a very large number to avoid repetition in the sequence. To obtain a uniform random number within a range in between l_1 and l_2 (where $l_2 > l_1$) linear scaling and point shifting are used and the random numbers in such intervals are generated as

$$\mathcal{Q}_i = l_1 + \mathcal{Q}_i(l_2 - l_1). \tag{42}$$

To generate a uniform sample in a two-dimensional (2D) triangular region, two independent random sequences are used as described in [40], [41], and [42]. Let us assume

u_1 and u_2 are two independent uniform random samples in between 0 to 1. So the uniform sample in the triangle can be generated by using the relation

$$\mathcal{Q}_i = d_1A + d_2B + d_3C, \tag{43}$$

where $d_1 = 1 - \sqrt{u_2}$, $d_2 = (1-u_1)\sqrt{u_2}$, and $d_3 = u_2\sqrt{u_1}$. A, B, and C are the column vectors that contain the coordinate of the vertices of a triangle in which we want to generate random points.

Similar to a triangle, a uniform random sample for a square/rectangle is generated by using the relation

$$\mathcal{Q}_i = d_1'A + d_2'B + d_3'C + d_4'D, \tag{44}$$

where $d_1' = u_1u_2$, $d_2' = u_1(1-u_2)$, $d_3' = (1-u_1)(1-u_2)$, and $d_4' = (1-u_1)u_2$. A, B, C, and D are the column vectors that contain the coordinate of the four corners of the rectangle or square.

The uniform random sample in a circular area centered at (x_c, y_c) having radius r is generated [43] by using the relation

$$\mathcal{Q}_i = \begin{bmatrix} x_c + ru_1 \cos 2\pi u_2 \\ y_c + ru_1 \sin 2\pi u_2 \end{bmatrix}. \tag{45}$$

Uniform random numbers inside a polygon can be generated by dividing it in many triangles and generating random samples proportional to the area of the triangle. A uniform random number for any arbitrary shape surface is generated by dividing the surface into triangles and circular arcs and generating proportionate uniform samples from each area. For a quite odd-shaped surface when it is not easy to divide it into well known geometric shapes, a sample rejection method [43] can be used to generate uniform random samples. In this method, the whole area is first covered with a rectangle or any other known geometric shape, and random samples are generated for that shape using the procedure discussed above. After sampling, we pick a sample if it is in our region of interest, otherwise, we go for another instance. This process is repeated until it generates the required number of samples.

REFERENCES

[1] S. C. Nardone and M. L. Graham, "A closed-form solution to bearings-only target motion analysis," *IEEE J. Ocean. Eng.*, vol. 22, no. 1, pp. 168–178, 1997.

[2] T. L. Song and J. L. Speyer, "The modified gain extended Kalman filter and parameter identification in linear systems," *Automatica*, vol. 22, no. 1, pp. 59–75, Jan. 1986.

[3] G. Hendeby, R. Karlsson, F. Gustafsson, and N. Gordon, "Recursive triangulation using bearings only sensors," in *Proc. IEE Seminar Target Tracking, Algorithms Appl.* London, U.K.: IET, Mar. 2006, pp. 3–10.

[4] L. Badriasl, S. Arulampalam, J. van der Hoek, and A. Finn, "Bayesian WIV estimators for 3-D bearings-only TMA with speed constraints," *IEEE Trans. Signal Process.*, vol. 67, no. 13, pp. 3576–3591, Jul. 2019.

[5] M. Beard and S. Arulampalam, "Comparison of data association algorithms for bearings-only multi-sensor multi-target tracking," in *Proc. 10th Int. Conf. Inf. Fusion*, Jul. 2007, pp. 1–7.

[6] Y. Oshman and P. Davidson, "Optimization of observer trajectories for bearings-only target localization," *IEEE Trans. Aerosp. Electron. Syst.*, vol. 35, no. 3, pp. 892–902, Jul. 1999.

[7] R. He, S. Chen, H. Wu, Z. Liu, and J. Chen, "Robust maneuver strategy of observer for bearings-only tracking," *Asian J. Control*, vol. 21, no. 4, pp. 1719–1731, Jul. 2019.

[8] S. Majumder, S. Scheding, and H. F. Durrant-Whyte, "Multisensor data fusion for underwater navigation," *Robot. Auto. Syst.*, vol. 35, no. 2, pp. 97–108, May 2001.

[9] M. Jacobi and D. Karimanzira, "Multi sensor underwater pipeline tracking with AUVs," in *Proc. OCEANS*, Sep. 2014, pp. 1–6.

[10] B. Sindhu, J. Valarmathi, and S. Christopher, "Bearing only target tracking using single and multisensor: A review," *J. Eng. Sci. Technol. Rev.*, vol. 12, no. 1, pp. 50–65, Feb. 2019.

[11] Y. Bar-Shalom and X.-R. Li, *Multitarget-Multisensor Tracking: Principles and Techniques*. Storrs, CT, USA: YBs, 1995.

[12] M. Mallick, V. Krishnamurthy, and B.-N. Vo, *Integrated Tracking, Classification, and Sensor Management*. Hoboken, NJ, USA: Wiley, 2012.

[13] R. Tharmarasa, T. Kirubarajan, and M. Hernandez, "Large-scale optimal sensor array management for multitarget tracking," *IEEE Trans. Syst., Man Cybern. C, Appl. Rev.*, vol. 37, no. 5, pp. 803–814, Sep. 2007.

[14] A. K. Gostar, R. Hoseinnezhad, and A. Bab-Hadiashar, "Robust multi-Bernoulli sensor selection for multi-target tracking in sensor networks," *IEEE Signal Process. Lett.*, vol. 20, no. 12, pp. 1167–1170, Dec. 2013.

[15] L. Weiss, A. Sanderson, and C. Neuman, "Dynamic sensor-based control of robots with visual feedback," *IEEE J. Robot. Autom.*, vol. RA-3, no. 5, pp. 404–417, Oct. 1987.

[16] S. Martínez and F. Bullo, "Optimal sensor placement and motion coordination for target tracking," *Automatica*, vol. 42, no. 4, pp. 661–668, Apr. 2006.

[17] S. Zhao, B. M. Chen, and T. H. Lee, "Optimal sensor placement for target localisation and tracking in 2D and 3D," *Int. J. Control*, vol. 86, no. 10, pp. 1687–1704, Oct. 2013.

[18] S. Xu and K. Doğançay, "Optimal sensor deployment for 3D AOA target localization," in *Proc. IEEE Int. Conf. Acoust., Speech Signal Process. (ICASSP)*, Apr. 2015, pp. 2544–2548.

[19] V. P. Dubey, R. K. Tiwari, and S. Bhaumik, "Selection of sensors during tracking a submarine," in *Proc. OCEANS*, Sep. 2021, pp. 1–6.

[20] E. Aarts, E. H. Aarts, and J. K. Lenstra, *Local Search in Combinatorial Optimization*. Princeton, NJ, USA: Princeton Univ. Press, 2003.

[21] R. Tharmarasa, T. Lang, and T. Kirubarajan, "Tracking with poorly localized sensors in multistatic sensor networks," *Proc. SPIE*, vol. 6969, Apr. 2008, pp. 202–211.

[22] H. Sun, M. Li, L. Zuo, and P. Zhang, "Resource allocation for multitarget tracking and data reduction in radar network with sensor location uncertainty," *IEEE Trans. Signal Process.*, vol. 69, pp. 4843–4858, 2021.

[23] A. Mishra, U. K. Sahoo, and S. Maiti, "Radio tomographic imaging with input sensor location uncertainty," in *Proc. Nat. Conf. Commun. (NCC)*, Feb. 2023, pp. 1–6.

[24] Z. Mao, H. Su, B. He, and X. Jing, "Moving source localization in passive sensor network with location uncertainty," *IEEE Signal Process. Lett.*, vol. 28, pp. 823–827, 2021.

[25] S. Haykin, *Kalman Filtering and Neural Networks*. Hoboken, NJ, USA: Wiley, 2004.

[26] I. Arasaratnam and S. Haykin, "Cubature Kalman filters," *IEEE Trans. Autom. Control*, vol. 54, no. 6, pp. 1254–1269, Jun. 2009.

[27] S. Bhaumik and Swati, "Cubature quadrature Kalman filter," *IET Signal Process.*, vol. 7, no. 7, pp. 533–541, Sep. 2013.

[28] E. A. Wan and R. Van Der Merwe, "The unscented Kalman filter for nonlinear estimation," in *Proc. Adapt. Syst. Signal Process., Commun., Control Symp.*, Oct. 2000, pp. 153–158.

[29] K. Ito and K. Xiong, "Gaussian filters for nonlinear filtering problems," *IEEE Trans. Autom. Control*, vol. 45, no. 5, pp. 910–927, May 2000.

[30] J. M. C. Clark, R. B. Vinter, and M. M. Yaqoob, "Shifted Rayleigh filter: A new algorithm for bearings-only tracking," *IEEE Trans. Aerosp. Electron. Syst.*, vol. 43, no. 99, pp. 1373–1384, 2007.

[31] R. Radhakrishnan, S. Bhaumik, and N. K. Tomar, "Gaussian sum shifted Rayleigh filter for underwater bearings-only target tracking problems," *IEEE J. Ocean. Eng.*, vol. 44, no. 2, pp. 492–501, Apr. 2019.

[32] Y. Bar-Shalom, X. R. Li, and T. Kirubarajan, *Estimation with Applications to Tracking and Navigation: Theory Algorithms and Software*. Hoboken, NJ, USA: Wiley, 2004.

[33] X. R. Li and V. P. Jilkov, "Survey of maneuvering target tracking. Part I. Dynamic models," *IEEE Trans. Aerosp. Electron. Syst.*, vol. 39, no. 4, pp. 1333–1364, Oct. 2003.

[34] K. Punithakumar, T. Kirubarajan, and M. Hernandez, "Multisensor deployment using PCRLBS, incorporating sensor deployment and motion uncertainties," *IEEE Trans. Aerosp. Electron. Syst.*, vol. 42, no. 4, pp. 1474–1485, Oct. 2006.

[35] Y. Guo, R. Tharmarasa, S. Rajan, T. L. Song, and T. Kirubarajan, "Passive tracking in heavy clutter with sensor location uncertainty," *IEEE Trans. Aerosp. Electron. Syst.*, vol. 52, no. 4, pp. 1536–1554, Aug. 2016.

[36] P. Tichavsky, C. H. Muravchik, and A. Nehorai, "Posterior Cramer–Rao bounds for discrete-time nonlinear filtering," *IEEE Trans. Signal Process.*, vol. 46, no. 5, pp. 1386–1396, May 1998.

[37] C. H. Papadimitriou and K. Steiglitz, *Combinatorial Optimization: Algorithms and Complexity*. North Chelmsford, MA, USA: Courier Corporation, 1998.

[38] X. R. Li, Z. Zhao, and V. P. Jilkov, "Practical measures and test for credibility of an estimator," in *Proc. Workshop Estimation, Tracking, Fusion*, 2001, pp. 481–495.

[39] C.-C. Li and B. Sun, "Using linear congruential generators for cryptographic purposes," in *Proc. Int. Conf. Comput. Appl.*, 2005, pp. 13–19.

[40] N. A. Smith and R. W. Tromble, "Sampling uniformly from the unit simplex," Dept. Comput. Sci., Johns Hopkins Univ., Baltimore, MD, USA, Tech. Rep. 29, 2004.

[41] C. Grimme, "Picking a uniformly random point from an arbitrary simplex," Inf. Syst. Statist., Munster, Germany, Tech. Rep., 2015, doi: 10.13140/RG.2.1.3807.6968.

[42] A. S. Glassner, *Graphics Gems*. Amsterdam, The Netherlands: Elsevier, 2013.

[43] G. Marsaglia, "Choosing a point from the surface of a sphere," *Ann. Math. Statist.*, vol. 43, no. 2, pp. 645–646, Apr. 1972.

VED PRAKASH DUBEY received the B.Tech. degree in electrical engineering from Dr. A. P. J. Abdul Kalam Technical University, Uttar Pradesh, Lucknow, in 2016, and the M.Tech. degree in electrical engineering from Aligarh Muslim University, Aligarh, in 2018. He is currently pursuing the Ph.D. degree with the Department of Electrical Engineering, Indian Institute of Technology Patna. He also worked on a project titled "Decentralized Consensus Filtering for Underwater Target Motion Analysis," funded by the Naval Research Board (NRB) of the Defence Research and Development Organization (DRDO) for around three years. His research interests include sensor fusion and nonlinear state estimation.

JOYDEB SAHA received the B.Tech. degree in electrical engineering from the Jalpaiguri Government Engineering College, West Bengal, in 2021. He is currently pursuing the Ph.D. degree with the Department of Electrical Engineering, Indian Institute of Technology Patna under the Prime Minister's Research Fellowship Scheme. His research interests include non-Gaussian state estimation and robust filtering.

SHOVAN BHAUMIK received the B.Sc. degree in physics from the University of Calcutta, in 1999, and the B.Tech. degree in electronics and instrumentation engineering and the M.E. and Ph.D. degrees in electrical engineering from Jadavpur University, in 2002, 2004, and 2009, respectively. From 2007 to 2009, he was a Research Engineer with the GE Global Research, GE India Technology Center, Bengaluru, India. He is currently an Associate Professor with the Department of Electrical Engineering, Indian Institute of Technology Patna. His research activities are supported by the Naval Research Board, Department of Science and Technology, Ministry of Electronics and Information Technology, and Defence Research and Development Organization, India. He has authored a book *Nonlinear Estimation Methods and Applications with Deterministic Sample Points* (CRC Press). His main research interests include nonlinear estimation, statistical signal processing, and underwater target tracking. He was a recipient of Young Faculty Research Fellowship Award from the Ministry of Electronics and Information Technology, Government of India.

ARITRO DEY (Member, IEEE) received the B.E. degree in electrical engineering, the M.E. degree in electrical engineering (specialization: control system), and the Ph.D. degree in electrical engineering (state and parameter estimation) from Jadavpur University, in 2008, 2011, and 2017, respectively. He is currently an Assistant Professor with the Department of Electrical Engineering, National Institute of Technology, Durgapur, West Bengal. His research interests include control systems, state and parameter estimation, and statistical signal processing.